Available online at www.sciencedirect.com
ScienceDirect
Trans. Nonferrous Met. Soc. China 30(2020) 3067−3077
Transactions of Nonferrous Metals Society of China
www.tnmsc.cn

Preparation and characterization of carbonyl iron soft magnetic composites with magnesioferrite insulating coating layer

Shi-geng LI[1,2], Ru-tie LIU[1], Xiang XIONG[1]

1. State Key Laboratory of Powder Metallurgy, Central South University, Changsha 410083, China;
2. Department of Materials and Chemistry Engineering, Pingxiang University, Pingxiang 337000, China

Received 24 October 2019; accepted 28 September 2020

Abstract: Spherical carbonyl iron (Fe) powders were coated with magnesioferrite ($MgFe_2O_4$) insulating coating layer and then mixed with epoxy-modified silicone resin (ESR). Soft magnetic composites (SMCs) were fabricated by compaction of the coated powders and annealing treatment. Transmission electron microscopy (TEM), scanning electron microscopy (SEM), energy dispersive spectroscopy (EDS), X-ray diffractometry (XRD) and X-ray photoelectron spectroscopy (XPS) revealed that the $MgFe_2O_4$ layer was coated on the surface of the iron powders. The magnetic properties of SMCs were determined using a vibrating sample magnetometer and an auto testing system for magnetic materials. The results showed that the SMCs prepared at 800 MPa and 550 °C exhibited a significant core loss of 167.5 W/kg at 100 kHz and 50 mT.

Key words: soft magnetic composites; in-situ oxidation preparation; magnesioferrite insulating coating layer; annealing treatment; magnetic properties

1 Introduction

Soft magnetic composites (SMCs) are widely applied in electrical reactors, transformers, filters, frequency modulation chokes and power supply owing to their excellent soft magnetic properties including high saturation magnetization, low coercivity and low core loss [1−3]. According to the application requirements, SMCs are designed and synthesized by smartly selecting metal magnetic particles and insulating coating materials [4,5]. The soft magnetic particles are generally pure Fe powders, Fe−Si alloys, Fe−Co alloys, Fe−Ni alloys, Fe−Si−Al alloys, Fe−Si−Ni alloys, Fe−Ni−Mo alloys, Fe−Si−B−P alloys and so on [6,7], each of which shows unique electromagnetic properties. Among these properties, it is critical to achieve low core loss to improve energy efficiency for applications in the medium and high frequency fields. Core loss mainly consists of hysteresis loss and eddy current loss. The eddy current loss is a significant component of the core loss at high frequency and can be greatly reduced by increasing the electrical resistivity of the SMCs. Lots of types of insulating materials have been used as the coating layer around the magnetic powders for increasing the electrical resistivity of the SMCs [8].

Generally, insulating layers are classified into the organic or inorganic coating. Organic materials including phenol-formaldehyde resin [9] and epoxy silicon resin [10] have been used to increase the electrical resistivity and enhance the mechanical strength of the SMCs. Inorganic materials such as oxides (e.g. Al_2O_3, SiO_2 and MgO) [11−14] and phosphates [15−17] are non-ferromagnetic, which reduce the saturation magnetization and improve the coercivity of the SMCs. Nevertheless, ferrite has unique properties such as high electrical resistivity and low eddy current loss, which should

Foundation item: Project (2016YFB0700302) supported by the National Key Research and Development Program of China; Projects (51862030, 51563020) supported by the National Natural Science Foundation of China
Corresponding author: Ru-tie LIU; Tel: +86-13974870967; E-mail: llrrtt@csu.edu.cn
DOI: 10.1016/S1003-6326(20)65443-7

be an appropriate insulating coating for the soft magnetic composites without any remarkable decrease in magnetic properties [18]. Furthermore, ferrite is commonly applied at higher and wider frequencies due to the low eddy current loss [19,20]. The spinel-type ferrite magnetic materials with the general formula of $M^{2+}(Fe^{3+})_2O_4$ (M^{2+}=Mg^{2+}, Mn^{2+}, Co^{2+}, Ni^{2+}, Cu^{2+}, Zn^{2+}, etc) have become an important area in nanoscience and nanotechnology, because of their huge applications in various fields such as biomedicine, magnetic materials, electronic materials, and photocatalyst [21−23]. Among various spinel ferrites, magnesium ferrite ($MgFe_2O_4$) has received great attention in the area of magnetic storage devices, microwave, and electronic devices because of its high magnetic permeability and high electrical resistance [24].

In this study, we have carefully fabricated uniform $MgFe_2O_4$ layer on the surface of Fe powder by in-situ oxidation. To the best of our knowledge, no studies have been reported on the use of $MgFe_2O_4$ as an insulating layer for carbonyl iron soft magnetic composites. The obtained coating powders were pressed and heat-treated to obtain the required SMCs. The characteristics of Fe/$MgFe_2O_4$ coated powders and microstructures of the SMCs after annealing treatment and magnetic properties were investigated. Moreover, the SMCs exhibited stable amplitude permeability and low core loss.

2 Experimental

2.1 Preparation of coated powders by in-situ oxidation method

The carbonyl iron powders with an average particle size of about 5.5 μm were supplied by Jiangxi Yuean Superfine Metal Co., Ltd. Magnesium chloride and ammonium hydroxide were from the Sinopharm Chemical Reagent Co., Ltd. $MgFe_2O_4$ insulating coating on the surface of Fe powder particles was produced by in-situ oxidation method. 100 g carbonyl iron powders were mixed with 300 mL different concentrations of $NH_3·H_2O$ (1.5, 2.5, 3.5 wt.%) with the addition of 2.03 g $MgCl_2·6H_2O$. The mixture was annealed at 180 °C for 1 h in an autoclave of 500 mL to complete in-situ oxidation reaction. The in-situ oxidized powders were then washed with deionized water and ethanol three times, prior to mixing with epoxy-modified silicone resin (ESR) (2 wt.%) dissolved in dimethyl benzene. The mixture was stirred at 80 °C until complete evaporation of the solution.

2.2 Composite preparation

The toroidal cores with an outer diameter of 26.1 mm, an inner diameter of 18.1 mm and a height of 4.5 mm were fabricated at a cold pressure of 800 MPa and room temperature. Then, the compacted cores were annealed at various temperatures (500−600 °C) for 1 h under Ar atmosphere to reduce the internal stress caused by pressing. The schematic diagram of the fabrication process of the Fe/$MgFe_2O_4$ soft magnetic composites is shown in Fig. 1.

2.3 Material characterization

The surface morphology of the oxidized Fe powders was observed by the transmission electron microscopy (TEM, JEM−2100F). The

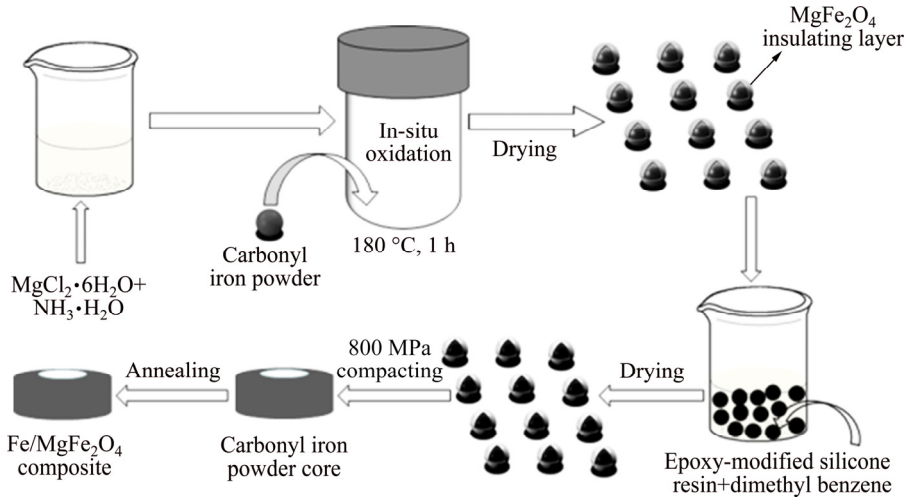

Fig. 1 Schematic diagram of fabrication process of Fe/$MgFe_2O_4$ soft magnetic composites

morphologies of the raw, insulating layer on the surface of Fe powders and annealed SMCs samples were examined using scanning electron microscopy (SEM) coupled with energy dispersive spectroscopy X-ray analysis (EDS, Hitachi SU8010). The phase identification of the Fe powders and the oxidized powders were analyzed by X-ray diffractometry (XRD, Advance D8) using Cu K_α radiation. The chemical state of the coating was analyzed by an X-ray photoelectron spectrometer (XPS, ESCALAB250Xi). Fourier transform infrared spectra (FT-IR) (Bruker VERTEX 70) were recorded in the wavenumber range from 400 to 4000 cm^{-1} at room temperature to investigate the composition of the insulating layer. Raman studies were performed in a LABRAM Aramis Raman microscopy system from Jobin Yvon France in the wavenumber range from 100 to 1000 cm^{-1} with a 532 nm laser. The thermal properties were examined by thermogravimetry and differential scanning calorimetry (TG−DSC, NETZSCH STA 449C), in which the samples were heated from room temperature to 700 °C under Ar atmosphere in alumina crucibles with a heating rate of 10 °C/min. The hysteresis loops were measured at room temperature by a vibrating sample magnetometer (VSM, Lake-shore 7400−s). The amplitude permeability and core loss of the SMCs were measured with a maximum applied magnetic induction of 50 mT over the frequency range from 10 to 170 kHz by an auto testing system (SY8258B-H/m) for magnetic materials.

3 Results and discussion

3.1 Microstructures

The typical TEM image of the oxidized Fe powders is shown in Fig. 2. The external gray coating layer was coated on the surface of the internal black part. The black part of Fe is confirmed to be coated with $MgFe_2O_4$. The generation mechanism of $MgFe_2O_4$ will be discussed in the following section.

Figures 3(a) and (b) show the morphologies of both the raw Fe particles and Fe powders oxidized with 2.5 wt.% $NH_3·H_2O$, respectively. Compared with the raw powders, the surface of the oxidized Fe powders was rougher, manifesting the formation of a coating layer after in-situ oxidation. SEM micrograph and EDS analysis of the coated powders after being polished are presented in Figs. 3(c−e). It can be obviously seen that the Fe powders were coated with a thin surface layer. The selected area 1 of the interior consists of iron and gold, while the selected area 2 of the coating layer obviously consists of magnesium, oxygen, iron and gold. Therefore, the $MgFe_2O_4$ layer has been formed. With respect to the analyzed depth, the comparison among the intensities of magnesium and iron peaks further confirms that the $MgFe_2O_4$ layer is thin. Gold appears in the EDS analysis as a result of the sample sprayed with gold.

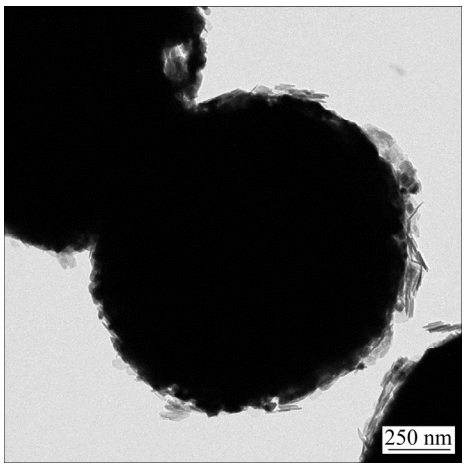

Fig. 2 TEM image of Fe/$MgFe_2O_4$ powders prepared with 2.5 wt.% $NH_3·H_2O$

The SEM image and EDS element distribution maps of the Fe powders coated with an insulating layer oxidized with 2.5 wt.% $NH_3·H_2O$ are shown in Fig. 4. Apparently, the $MgFe_2O_4$ layer was completely and uniformly covered on the surface of the Fe powders, which is the key to ensure the relatively low eddy current loss of the SMCs. Moreover, the elemental distribution maps revealed that Mg, O and Fe were uniformly distributed on the surface of the Fe powder particles. It can be inferred that each particle was coated by a uniform and thin insulating layer.

3.2 XRD patterns

XRD analysis has been implemented to identify the phase composition of the coating. Figure 5 shows the XRD patterns of the raw Fe powders and those oxidized with different $NH_3·H_2O$ concentrations (1.5, 2.5, 3.5 wt.%). The diffraction peaks at 2θ values of 44.70°, 65.03° and 82.36° were assigned to the (110), (200) and (211) planes of Fe (JCPDS No. 87-0721). Additional

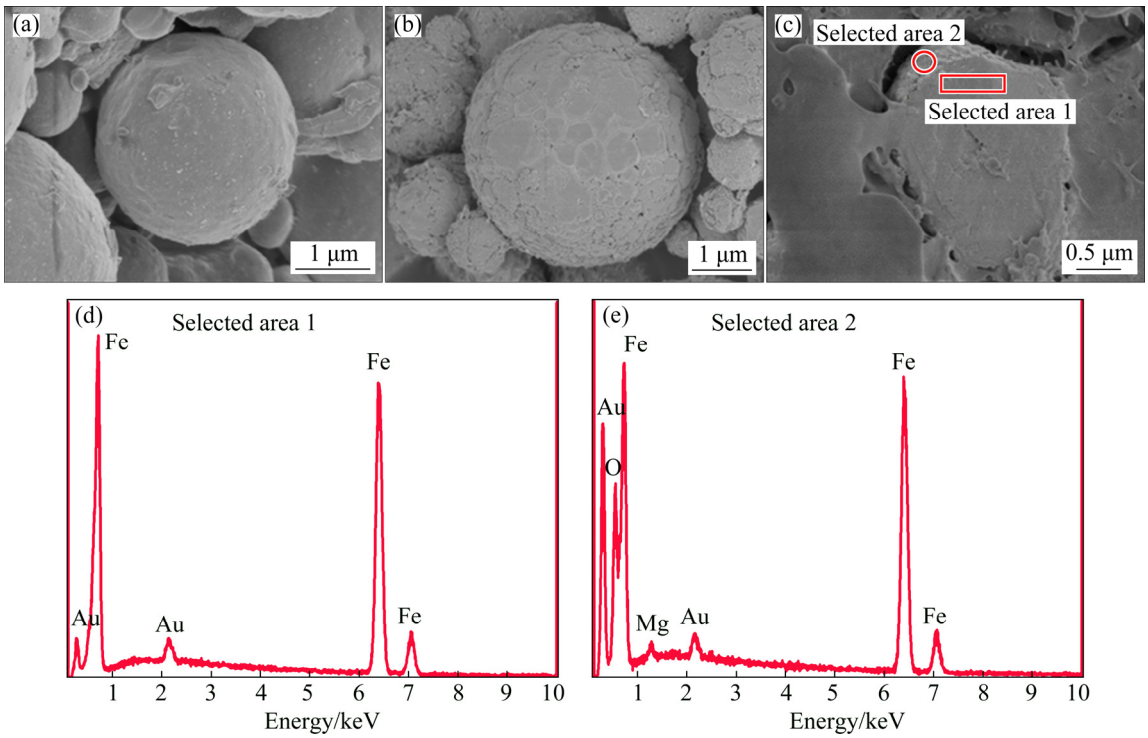

Fig. 3 SEM images of raw (a) and oxidized (b) Fe powders, EDS spectrum of polished oxidized Fe powders (c) with EDS analysis of selected areas 1 (d) and 2 (e) in (c)

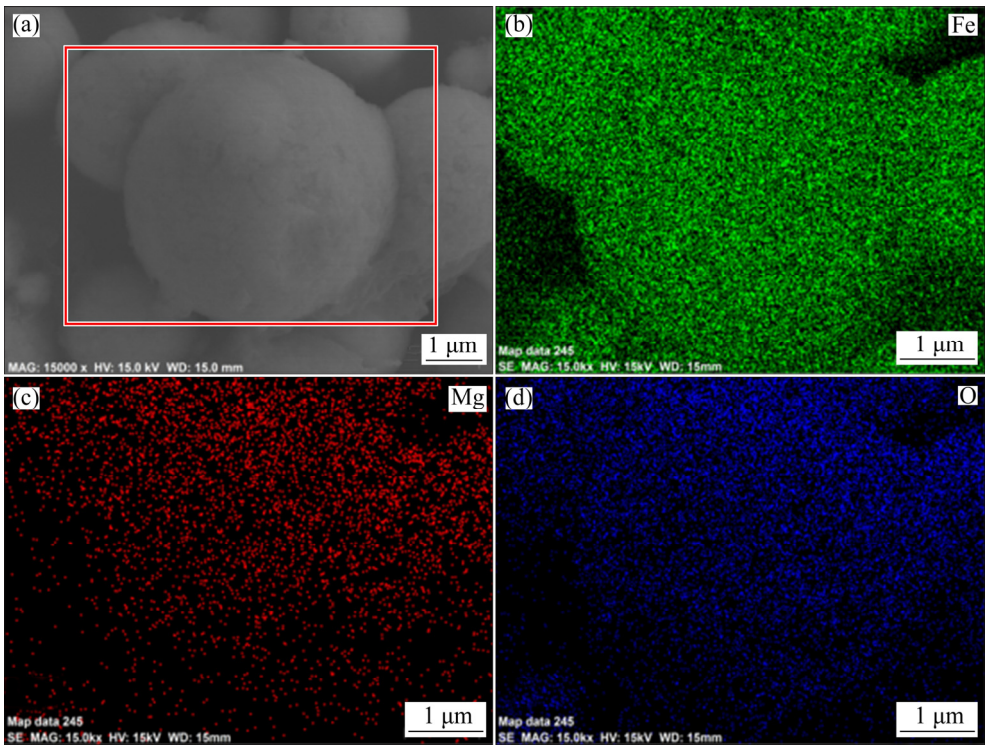

Fig. 4 SEM image (a) and EDS elemental distribution maps (b−d) of Fe/$MgFe_2O_4$ composite powders

characteristic peaks appeared at 2θ values of 35.39° and 62.56° for the surface-oxidized Fe powders, corresponding to the (311) and (440) planes of the $MgFe_2O_4$ (JCPDS No. 88-1935) [21,25]. No peak of any other phase was detected. The intensity ratio between the $MgFe_2O_4$ and Fe main peaks increases with increasing ammonia concentration, indicating the formation of thicker $MgFe_2O_4$.

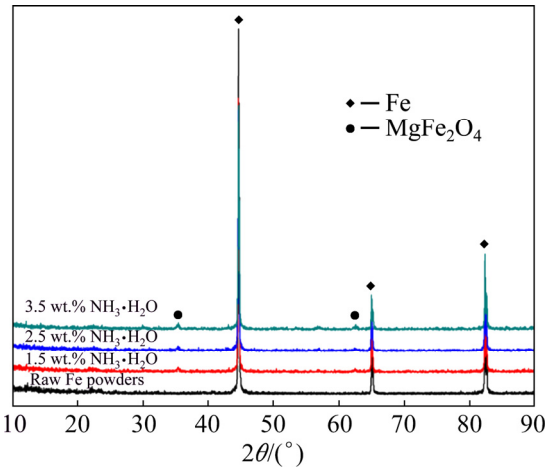

Fig. 5 XRD patterns of raw Fe powders and those oxidized with different $NH_3·H_2O$ concentrations

3.3 XPS spectra

In order to further investigate the oxidation state of the coating layer, the XPS test was performed for the oxidized powders. Figure 6 shows the XPS spectra of the oxidized Fe powders after Ar^+ sputtering for 1000 s. Detailed XPS spectra of the Mg 1s and the Fe 2p peaks are shown in Figs. 6(a) and (b), respectively. The Mg 1s peak located at around 1303.3 eV is observed in the XPS spectrum which corresponds to Mg^{2+}. Two main peaks, Fe $2p_{1/2}$ and Fe $2p_{3/2}$ located at around 724.3 and 710.9 eV are observed in the XPS spectra, respectively. Additionally, a weak satellite peak at ~719 eV is observed in the XPS spectrum which corresponds to Fe^{3+} [26−28]. No peak corresponding to the metallic Fe is observed, suggesting the formation of a complete oxide coating layer. Figure 6(c) shows a survey spectrum of the oxidized powders, indicating the existence of magnesium, iron and oxygen. Experimental results of XPS measurement further demonstrate the oxidation layer composition of $MgFe_2O_4$.

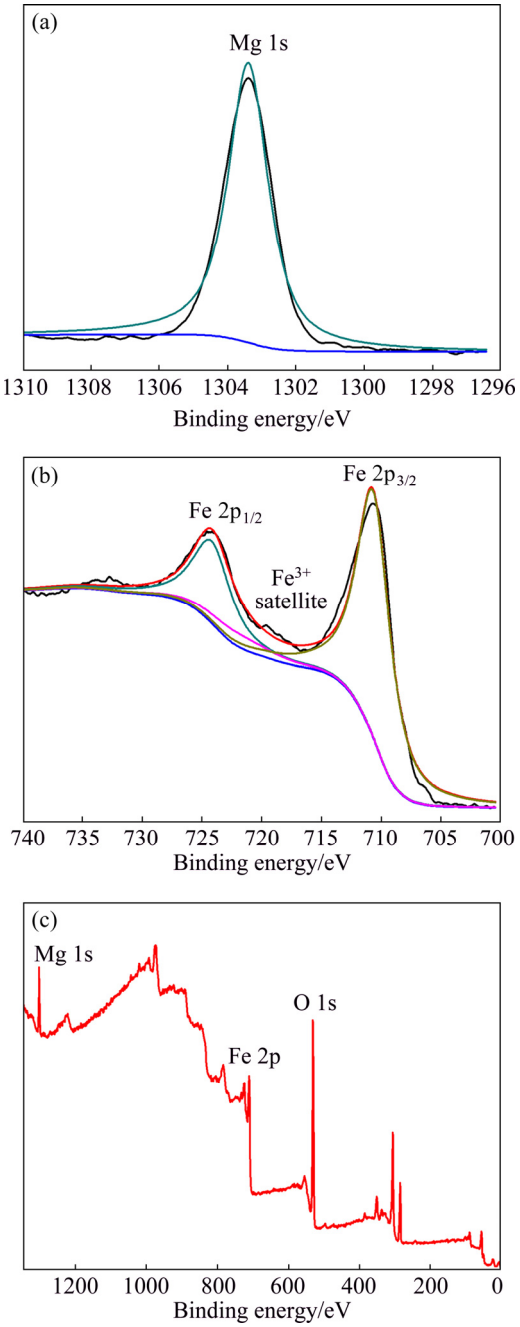

Fig. 6 XPS spectra of Mg 1s (a), Fe 2p (b) and survey XPS spectrum (c) of Fe powders oxidized with 2.5 wt.% $NH_3·H_2O$

3.4 FT-IR and Raman spectra

In addition, the FT-IR spectrum in the range of 400−4000 cm^{-1} was used to characterize the oxidized Fe powders, as shown in Fig. 7. The broad absorption bands due to the —OH vibration are observed at 3420, 1634, 1396 and 1030 cm^{-1}, due to adsorbed water on the surface. The spectrum of the oxidized Fe powders reveals the absorption band at 592 cm^{-1}, which is assigned to the Fe—O stretching band. The small absorption band at around 448 cm^{-1} may be assigned to the Mg—O stretching vibration mode [29−31], which is attributed to the existence of $MgFe_2O_4$, confirming that the $MgFe_2O_4$ insulating layer was successfully coated on the surface of Fe powders.

Raman spectrum of Fe/$MgFe_2O_4$ composites was collected in the range of 100−1000 cm^{-1}, as shown in Fig. 8. The recorded spectrum of the

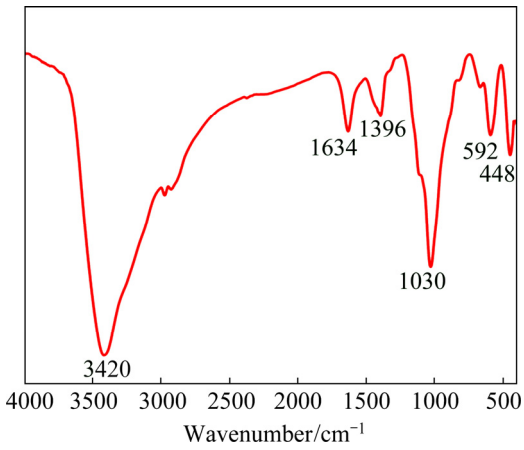

Fig. 7 FT-IR spectrum of oxidized Fe powders prepared with 2.5 wt.% $NH_3·H_2O$

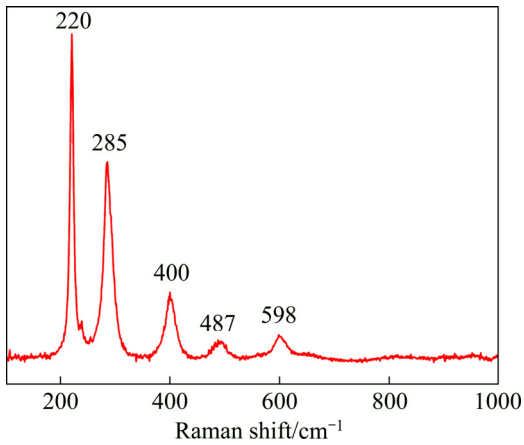

Fig. 8 Raman spectrum of Fe/$MgFe_2O_4$ composites

$MgFe_2O_4$ shows five expected Raman active modes E_g at 285 and 400 cm^{-1} and $3F_{2g}$ at 220, 487 and 598 cm^{-1} [32−34]. For the division of peaks, the literature is inconsistent. The Raman bands observed at 220, 285 and 487 cm^{-1} could be attributed to the $F_{2g}(1)$, E_g and $F_{2g}(2)$ Raman modes involving motion of the Fe^{3+} and those at 400 and 598 cm^{-1} could be assigned to the E_g and $F_{2g}(3)$ Raman modes involving motion of the Mg^{2+}, respectively.

Based on the above-mentioned results, the in-situ oxidation mechanism can be deduced. The reactions for the formation of $MgFe_2O_4$ can be expressed in the following equations. According to the Pourbaix diagram [35], Fe reacts with H_2O to form $Fe(OH)_2$ and is further oxidized to be $[Fe(OH)_n]^{-(n-3)}$ (n=2, 3) by the small amount of dissolved O_2 in solution. $Mg(OH)_2$ will form quickly because Mg^{2+} is rendered in an ammonia solution. Finally, the newly formed $Mg(OH)_2$ will react with hydroxy complexes $[Fe(OH)_n]^{-(n-3)}$ to form ferromagnetic $MgFe_2O_4$ [36]:

$$Fe+2H_2O \rightarrow Fe(OH)_2+H_2\uparrow \quad (1)$$

$$Fe(OH)_2+OH^-+O_2+H_2O \rightarrow [Fe(OH)_n]^{-(n-3)} \quad (n=2, 3) \quad (2)$$

$$Mg^{2+}+2OH^- \rightarrow Mg(OH)_2 \quad (3)$$

$$Mg(OH)_2+[Fe(OH)_n]^{-(n-3)} \rightarrow MgFe_2O_4 \quad (4)$$

3.5 TG−DSC curves

Aiming to study the thermal stability of the coating, TG−DSC analysis was executed by heating the $MgFe_2O_4$/ESR-coated Fe powders in the temperature range from 30 to 700 °C on a NETZSCH STA 449C, under Ar atmosphere in alumina crucibles with a heating rate of 10 °C/min. An apparently decrease in the mass was observed at about 200 °C due to the thermal degradation of the ESR layer in Fig. 9. The ESR layer decomposes slowly with the temperature increasing. When mass fraction of ESR in the SMCs is 2%, the mass loss of SMCs powders is merely 1.12% at 700 °C.

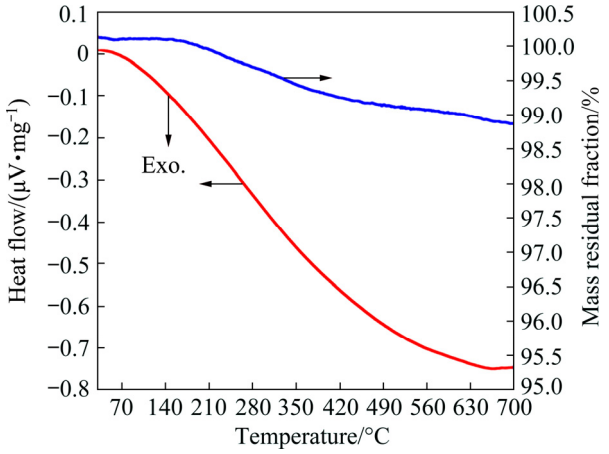

Fig. 9 TG−DSC curves of Fe powders coated with $MgFe_2O_4$/ESR

All the above results revealed that the Fe powders were coated with $MgFe_2O_4$. Then, the ESR was coated on the oxidized Fe particles constructing inorganic−organic hybrid insulating layer. The outstanding and unique $MgFe_2O_4$ insulating layer on the surface of Fe powders is the key to manufacture SMCs with the excellent property.

3.6 Hysteresis loops

The hysteresis loops of the Fe powders and those undergoing different reaction concentrations

were measured by VSM. Figure 10 shows the saturated magnetization (M_s) as a function of the magnetic field strength ranging from −1600 to 1600 kA/m. The saturated magnetization (M_s) values decrease gradually from 1654 to 1600 A/m with increasing ammonia concentration, which can be explained by the insulating layer of $MgFe_2O_4$ with lower M_s [37]. These M_s values of the oxidized Fe powders bring into correspondence with the raw Fe powders (1677 A/m) as shown in the inset in Fig. 10. This is attributed to the formation of the ferromagnetic $MgFe_2O_4$ coating by the in situ oxidation method for the prevention of magnetic dilution.

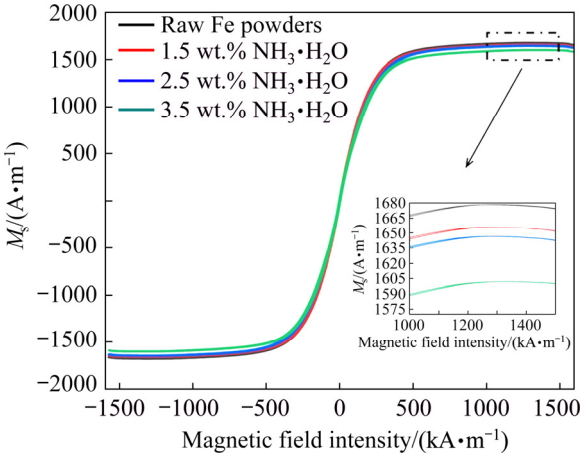

Fig. 10 Hysteresis loops for raw Fe powders and those oxidized with different $NH_3·H_2O$ concentrations

3.7 Microstructures after heat treatment

The cross-section SEM images and the element distributions of the samples oxidized with 2.5 wt.% $NH_3·H_2O$ after annealing treatment at 500 °C for 1 h in the Ar atmosphere are shown in Fig. 11. The complete and uniform insulation layer is still coated on the surface of the Fe particles after the annealing treatment. The gold appears in the EDS analysis due to the sample sprayed with gold. The large particles are pure Fe and do not contain other elements (Figs. 11(a_1, a_2); coating layer (dark part) of the particles contains Fe, O, Mg and Si, (Fig. 11(b_1, b_2)). Because of the thin $MgFe_2O_4$ layer, the intensities of the Mg are significantly weaker than those of Fe.

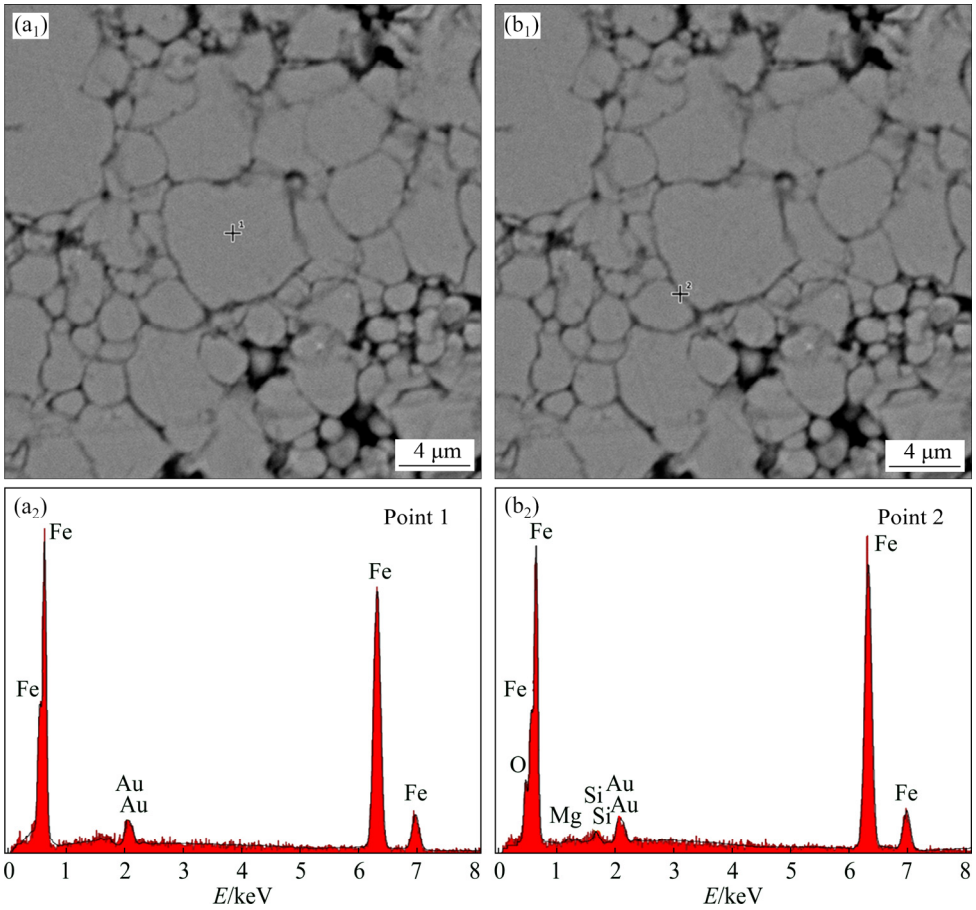

Fig. 11 Cross-section SEM images (a_1, b_1) and element distributions (a_2, b_2) of samples oxidized with 2.5 wt.% $NH_3·H_2O$ after annealing treatment at 500 °C for 1 h in Ar atmosphere

3.8 Effect annealing temperature on magnetic properties of SMCs

Figure 12 shows the amplitude permeability (μ_a) dependence on the frequency for Fe SMCs annealed at different temperatures, and oxidized with different ammonia concentrations and annealed at 550 °C. It can be seen that all the Fe SMCs exhibit good frequency stability of μ_a from 10 kHz to 170 kHz. The μ_a of the Fe SMCs increases slightly when the annealing temperature is raised from 500 to 550 °C. This phenomenon can be explained that annealing treatment can reduce the distortions within the particles, lower the residual stress, and improve the heat expansion coefficient of iron particles. Clearly, when the annealing temperature increases from 550 to 600 °C, the μ_a decreases slightly due to the decomposition of the organic insulating layer to form pores.

Figure 13 shows core loss (P_s) as a function of frequency for Fe SMCs annealed at different temperatures and oxidized with different $NH_3{\cdot}H_2O$ concentrations after annealing at 550 °C. The P_s of the SMCs mainly consists of the hysteresis loss P_h and eddy current loss P_e, given by the following equation [20,38]:

$$P_s = P_h + P_e = f\oint H\mathrm{d}B + \frac{CB^2 f^2 d^2}{\rho} \tag{5}$$

where f is the frequency, H is the magnetic field intensity, B is the flux density, C is proportionality constant, d is the thickness of the material and ρ is the resistivity of the material. Hence, with an increase in frequency, P_s grows rapidly. P_e can be divided into two different components: in-particle, which originates from eddy current loss inside the particle, and inter-particle, which is caused by insulating between the particles [1]. When the insulating layer of the sample is not damaged, the effect of annealing treatment on the eddy current loss is quite small. The core loss measured at 100 kHz and 50 mT decreases from 190.3 to 167.5 W/kg as the annealing temperature changes

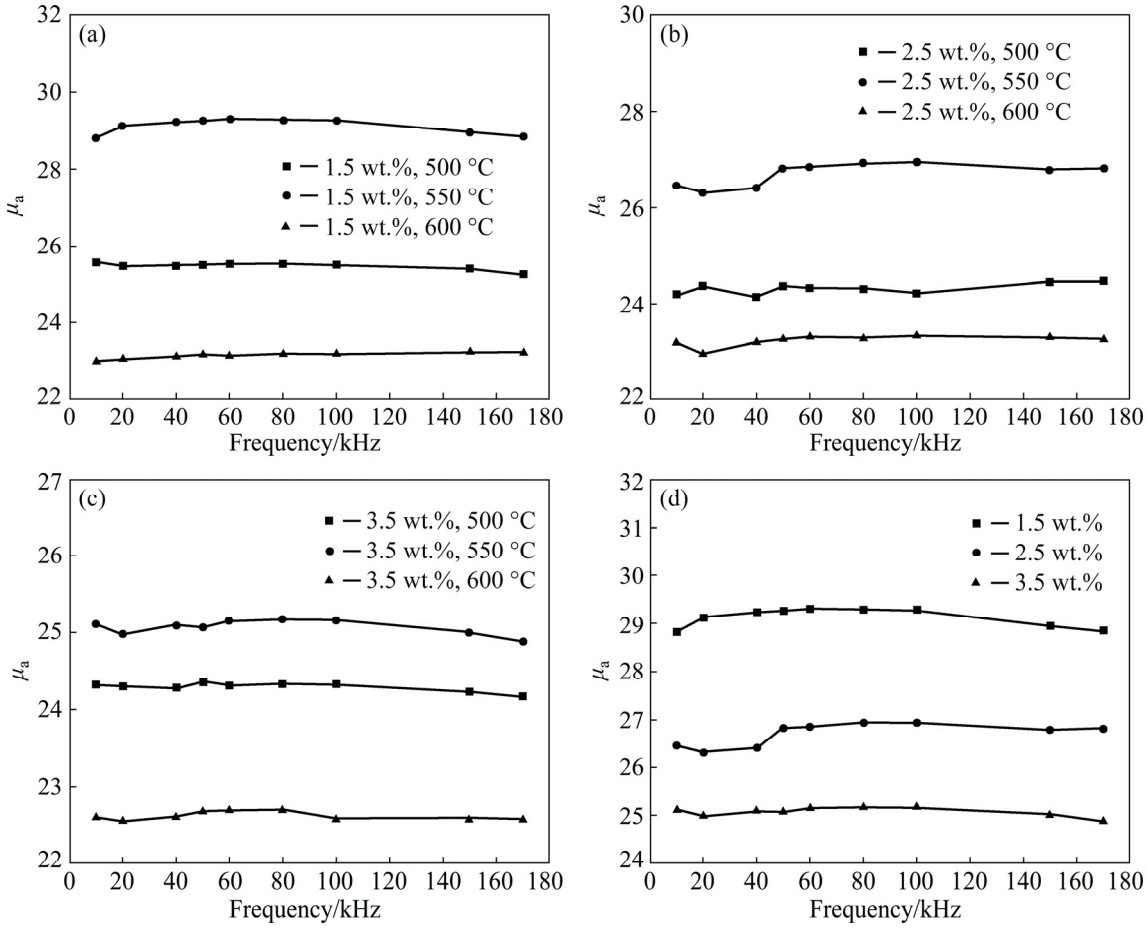

Fig. 12 Amplitude permeability (μ_a) dependence on frequency of Fe SMCs prepared with $NH_3{\cdot}H_2O$ concentrations of 1.5 wt.% (a), 2.5 wt.% (b), 3.5 wt.% (c) and annealed at different temperatures, and of those prepared with different ammonia concentrations at annealing temperature of 550 °C (d)

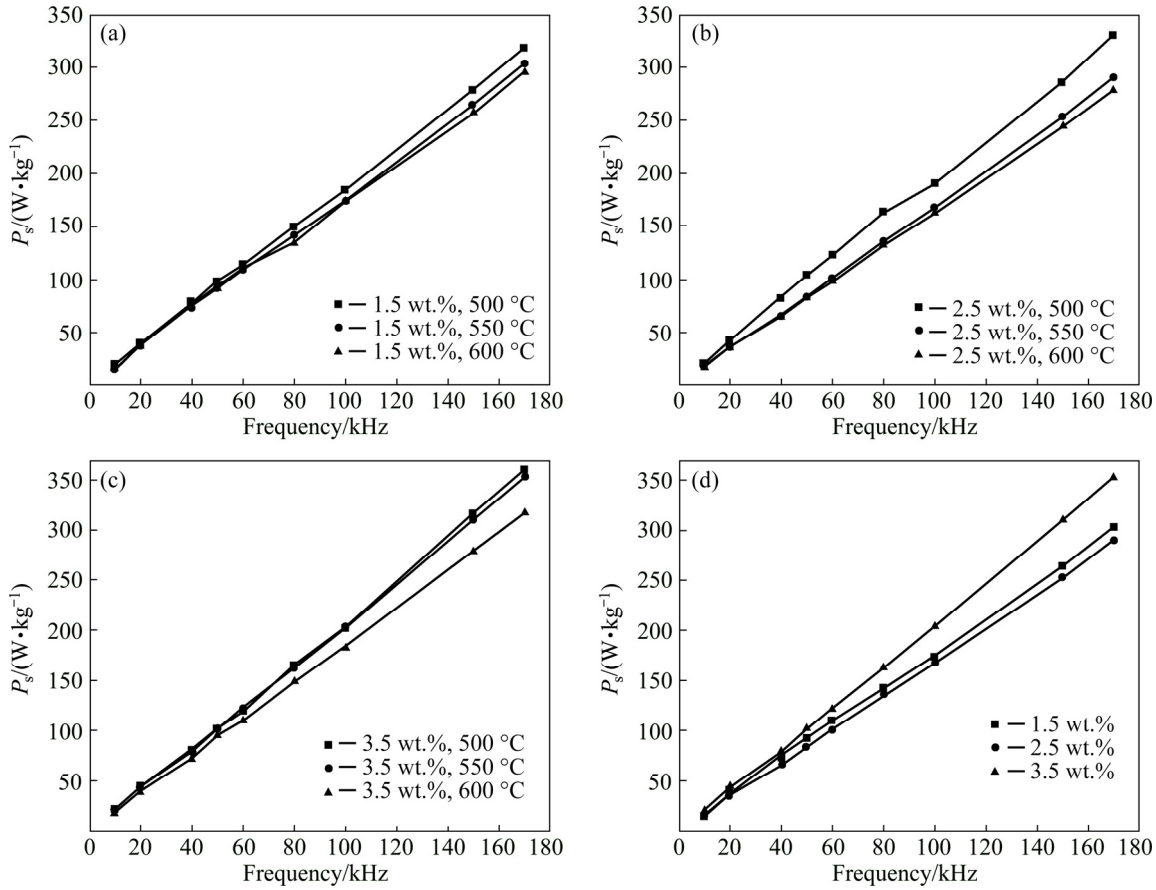

Fig. 13 Core loss−frequency curves of Fe SMCs prepared with different ammonia concentrations of 1.5 wt.% (a), 2.5 wt.% (b), 3.5 wt.% (c) and annealed at different temperatures, and of those and prepared with different ammonia concentrations at annealing temperature of 550 °C (d)

from 500 to 550 °C, as shown in Fig. 13(b). The internal stress is not completely eliminated at 500 °C, which causes the hysteresis loss to be high. When the annealing temperature ranges from 550 to 600 °C, the core loss decreases slightly from 167.5 to 162.1 W/kg. It can be explained by the internal stress which is completely eliminated at 550 °C. This can reduce the hysteresis loss. Therefore, 550 °C is the most suitable annealing temperature for the Fe SMCs. Figure 13(d) shows the core loss of the samples annealed at 550 °C with $NH_3·H_2O$ concentration ranging from 1.5 to 3.5 wt.%. The minimum core loss of 167.5 W/kg measured at 100 kHz is achieved with $NH_3·H_2O$ concentration of 2.5 wt.%. When $NH_3·H_2O$ concentration is 1.5 wt.%, the very thin $MgFe_2O_4$ insulating layer is insufficient to provide large electrical resistivity for the SMCs, which results in large eddy current loss. Based on the above discussion, it can be indicated that the optimal magnetic performance can be obtained at 550 °C with $NH_3·H_2O$ concentration of 2.5 wt.%.

4 Conclusions

(1) Soft magnetic composites containing Fe powders coated with $MgFe_2O_4$ insulating layer were prepared via in-situ oxidation method. The TEM analysis shows that a thin and uniform layer was coated on the surface of the Fe powders. The SEM, EDS, XRD, XPS, FT-IR and Raman analysis results indicated that the chemical composition of the coating layer is $MgFe_2O_4$. The $MgFe_2O_4$ layer has effectively enhanced the magnetic properties of Fe SMCs with significant low core loss.

(2) The core loss of 167.5 W/kg at 100 kHz and 50 mT is obtained for the SMCs made of Fe powders in-situ oxidized with $NH_3·H_2O$ concentration of 2.5 wt.% after annealing at 550 °C. This study provides a promising approach to achieve low core loss for other Fe-based SMCs.

References

[1] SHOKROLLAHI H, JANGHORBAN K. Soft magnetic composite materials (SMCs) [J]. Journal of Materials Processing Technology, 2007, 189: 1−12.

[2] QIAN L W, PENG J G, XIANG Z, PAN Y F, LU W. Effect of annealing on magnetic properties of Fe/Fe_3O_4 soft magnetic composites prepared by in-situ oxidation and hydrogen reduction methods [J]. Journal of Alloys and Compounds, 2019, 778: 712−720.

[3] PENG Y D, YI Y, LI L Y, AI H Y, WANG X X, CHEN L L. Fe-based soft magnetic composites coated with NiZn ferrite prepared by a co-precipitation method [J]. Journal of Magnetism and Magnetic Materials, 2017, 428: 148−153.

[4] DIAS M M, MOZETIC H J, BARBOZA J S, MARTINS R M, PELEGRINI L, SCHAEFFER L. Influence of resin type and content on electrical and magnetic properties of soft magnetic composites (SMCs) [J]. Powder Technology, 2013, 237: 213−220.

[5] LI W C, WANG Z J, YING Y, YU J, ZHENG J W, QIAO L, CHE S L. In-situ formation of Fe_3O_4 and ZrO_2 coated Fe-based soft magnetic composites by hydrothermal method [J]. Ceramic International, 2019, 45: 3864−3870.

[6] PERSSON M. Development in soft magnetic components [J]. Metal Powder Report, 2000, 55: 10−11.

[7] LI X L, DONG Y Q, LIU M, CHANG C T, WANG X M. New Fe-based amorphous soft magnetic composites with significant enhancement of magnetic properties by compositing with nano-(NiZn)Fe_2O_4 [J]. Journal of Alloys and Compounds, 2017, 696: 1323−1328.

[8] HUANG M Q, WU C, JIANG Y Z, YAN M. Evolution of phosphate coatings during high-temperature annealing and its influence on the Fe and FeSiAl soft magnetic composites [J]. Journal of Alloys and Compounds, 2015, 644: 124−130.

[9] KOLLAR P, BIRCAKOVA Z, FUEZER J, BURES R, FABEROVA M. Power loss separation in Fe-based composite materials [J]. Journal of Magnetism and Magnetic Materials, 2013, 327: 146−150.

[10] XIAO L, SUN Y H, DING C H, YANG L H, YU L. Annealing effects on magnetic properties and strength of organic-silicon epoxy resin-coated soft magnetic composites [J]. Journal Mechanical Engineering Science, 2014, 228: 2049−2058.

[11] LUO F, FAN X, LUO Z G, HU W T, LI G Q, LI Y W, LIU X, WANG J. Ultra-low inter-particle eddy current loss of Fe_3Si/Al_2O_3 soft magnetic composites evolved from FeSiAl/Fe_3O_4 core-shell particles [J]. Journal of Magnetism and Magnetic Materials, 2019, 484: 218−224.

[12] LEI J, ZHENG J W, ZHENG H D, QIAO L, YING Y, CAI W, LI W C, YU J, LIN M, CHE S L. Effects of heat treatment and lubricant on magnetic properties of iron-based soft magnetic composites with Al_2O_3 insulating layer by one-pot synthesis method [J]. Journal of Magnetism and Magnetic Materials, 2019, 472: 7−13.

[13] LUO Z G, FAN X A, HU W T, LUO F, LI G Q, LI Y W, LIU X, WANG J. Controllable SiO_2 insulating layer and magnetic properties for intergranular insulating Fe−6.5wt.%Si/SiO_2 composites [J]. Advanced Powder Technology, 2019, 30: 538−543.

[14] ZHANG Y, ZHOU T D. Structure and electromagnetic properties of FeSiAl particles coated by MgO [J]. Journal of Magnetism and Magnetic Materials, 2017, 426: 680−684.

[15] XIA C, PENG Y D, YI Y, DENG H, ZHU Y Y, HU G. The magnetic properties and microstructure of phosphated amorphous FeSiCr/silane soft magnetic composite [J]. Journal of Magnetism and Magnetic Materials, 2019, 474: 424−433.

[16] OIKONOMOU C, HRYHA E, NYBORG L. Development of methodology for surface analysis of soft magnetic composite powders [J]. Surface and Interface Analysis, 2012, 44: 1166−1170.

[17] CHEN Z H, LIU X S, KAN X C, WANG Z, ZHU R W, YANG W, WU Q Y, SHEZAD M. Phosphate coatings evolution study and effects of ultrasonic on soft magnetic properties of FeSiAl by aqueous phosphoric acid solution passivation [J]. Journal of Alloys and Compounds, 2019, 783: 434−440.

[18] XIE D S, LIN K H, LIN S T. Effects of processed parameters on the magnetic performance of a powder magnetic core [J]. Journal of Magnetism and Magnetic Materials, 2014, 353: 34−40.

[19] KANG E Y, CHUNG Y H. Surface oxidation and magnetic properties of Fe−Si−B−Nb amorphous alloy [J]. IEEE Transactions on Magnetics, 2009, 45: 2597−2600.

[20] KALARUS J, KOGIAS G, HOLZ D, ZASPALIS V T. High permeability-high frequency stable MnZn ferrites [J]. Journal of Magnetism and Magnetic Materials, 2012, 324: 2788−2794.

[21] MANIKANDAN A, DURKA M, SEEVAKAN K, ARUL ANTONY S. A novel one-pot combustion synthesis and opto-magnetic properties of magnetically separable spinel $Mn_xMg_{1-x}Fe_2O_4$ ($0.0\leq x\leq 0.5$) nanophotocatalysts [J]. Journal of Superconductivity and Novel Magnetism, 2015, 28: 1405−1416.

[22] RAVICHANDRAN A T, SRINIVAS J, KARTHICK R, MANIKANDAN A, BAYKAL A. Facile combustion synthesis, structural, morphological, optical and antibacterial studies of $Bi_{1-x}Al_xFeO_3$ ($0.0 \leq x \leq 0.15$) nanoparticles [J]. Ceramics International, 2018, 44: 13247−13252.

[23] ARUL MARY J, MANIKANDAN A, JOHN KENNEDY L, BOUOUDINA M, SUNDARAM R, JUDITH VIJAYA J. Structure and magnetic properties of Cu−Ni alloy nanoparticles prepared by rapid microwave combustion method [J]. Transactions of Nonferrous Metals Society of China, 2014, 24: 1467−1473.

[24] GODLYN ABRAHAM A, MANIKANDAN A, MANIKANDAN E, VADIVEL S, JAGANATHAN S K, BAYKAL A, SRI RENGANATHAN P. Enhanced magneto-optical and photo-catalytic properties of transition metal cobalt (Co^{2+} ions) doped spinel $MgFe_2O_4$ ferrite nano-composites [J]. Journal of Magnetism and Magnetic Materials, 2018, 452: 380−388.

[25] PRADEEP A, PRIYADHARSINI P, CHANDRASEKARAN G. Sol−gel route of synthesis of nanoparticles of $MgFe_2O_4$ and XRD, FTIR and VSM study [J]. Journal of Magnetism and Magnetic Materials, 2008, 320: 2774−2779.

[26] ZHAO G L, WU C, YAN M. Fe-based soft magnetic composites with high Bs and low core loss by acidic bluing coating [J]. IEEE Transactions on Magnetics, 2015, 51: 1−4.
[27] YAMASHITA T, HAYES P. Analysis of XPS spectra of Fe^{2+} and Fe^{3+} ions in oxide materials [J]. Applied Surface Science, 2008, 254: 2441−2449.
[28] GROSVENOR A P, KOBR B A, BIESINGER M C, MCLNTYRE N S. Investigation of multiplet splitting of Fe 2p XPS spectra and bonding in iron compounds [J]. Surface Interface Analysis, 2004, 36: 1564−1574.
[29] ZHANG D, ZHU M Y, YU J G, MENG H W, JIAO F P. Effective removal of brilliant green from aqueous solution with magnetic Fe_3O_4@SDBS@LDHs composites [J]. Transactions of Nonferrous Metals Society of China, 2017, 27: 2673−2681.
[30] KAUR J, KAUR M. Facile fabrication of ternary nanocomposite of $MgFe_2O_4$−TiO_2@GO for synergistic adsorption and photocatalytic degradation studies [J]. Ceramic International, 2019, 45: 8646−8659.
[31] SUGUNA S, SHANKAR S, JAGANATHAN S K, MANIKANDAN A. Novel synthesis and characterization studies of spinel $Ni_xCo_{1-x}Al_2O_4$ (x=0.0 to 1.0) nano-catalysts for the catalytic oxidation of benzyl alcohol [J]. Journal of Nanoscience and Nanotechnology, 2018, 18: 1019−1026.
[32] CHEN W, LIU Q Y, ZHU X X, FU M. One-step in situ growth of magnesium ferrite nanorods on graphene and their microwave-absorbing properties [J]. Applied Organometallic Chemistry, 2018, 32: e4017.
[33] D'IPPOLITO V, ANDREOZZI G B, BERSANI D, LOTTICI P P. Raman fingerprint of chromate, aluminate and ferrite spinels [J]. Journal of Raman Spectroscopy, 2015, 46: 1255−1264.
[34] LEKHA P C, RAMESH G, REVATHI V, SUBRAMANIAN V. Relaxor-like ferroelectric behavior favoured by short-range B-site ordering in 10% Ba^{2+} substituted $MgFe_2O_4$ [J]. Materials Research Bulletin, 2014, 53: 240−245.
[35] POURBAIX M. Atlas of electrochemical equilibria in aqueous solution [M]. 2nd ed. Houston: National Association of Corrosion Engineers, 1974.
[36] YU S H, YOSHIMURA M. Direct fabrication of ferrite MFe_2O_4 (M=Zn, Mg)/Fe composite thin films by soft solution processing [J]. Chemistry of Materials, 2000, 12: 3805−3810.
[37] CHINNASAMY C N, NARAYANASAMY A, PONPANDIAN N, CHATTOPADHYAY K. The influence of Fe^{3+} ions at tetrahedral sites on the magnetic properties of nanocrystalline $ZnFe_2O_4$ [J]. Materials Science and Engineering A, 2001, 304: 983−987.
[38] LI S G, LIU R T, XIONG X. Fe-based soft magnetic composites with high permeability and low core loss by in situ coating $ZnFe_2O_4$ layer [J]. Journal of Materials Science, 2020, 55: 274−282.

铁酸镁绝缘包覆羰基铁粉软磁复合材料的制备与性能表征

李石庚[1,2]，刘如铁[1]，熊 翔[1]

1. 中南大学 粉末冶金国家重点实验室，长沙 410083；
2. 萍乡学院 材料与化学工程学院，萍乡 337000

摘 要：球形羰基铁粉颗粒经铁酸镁($MgFe_2O_4$)绝缘包覆后，与改性环氧有机硅树脂(ESR)均匀混合，通过压制成型和退火处理制得软磁复合材料。TEM、SEM、EDS、XRD 和 XPS 分析结果表明，$MgFe_2O_4$ 层包覆在铁粉颗粒表面。采用振动样品磁强计和磁性材料自动测试系统对样品进行磁性能测试。经 800 MPa 压制和 550 °C 退火处理后软磁复合材料在 100 kHz 和 50 mT 时的磁芯损耗为 167.5 W/kg。

关键词：软磁复合材料；原位氧化制备；铁酸镁绝缘涂层；退火处理；磁性能

(Edited by Wei-ping CHEN)